

Highly sensitive electromechanical piezoresistive pressure sensors based on large-area layered PtSe₂ films

*Stefan Wagner¹, Chanyoung Yim², Niall McEvoy³, Satender Kataria¹, Volkan Yokaribas⁴,
Agnieszka Kuc⁵, Stephan Pindl⁶, Claus-Peter Fritzen⁴, Thomas Heine⁵, Georg S. Duesberg³,
Max C. Lemme^{1,7*}*

¹Chair of Electronic Devices, Faculty of Electrical Engineering and Information Technology, RWTH Aachen University, Otto-Blumenthal-Str. 2, 52074 Aachen, Germany

²Institute of Physics, EIT 2, Faculty of Electrical Engineering and Information Technology, Universität der Bundeswehr München, Werner-Heisenberg-Weg 39, 85577 Neubiberg, Germany

³Centre for Research on Adaptive Nanostructures and Nanodevices (CRANN), Advanced Materials and BioEngineering Research (AMBER) and School of Chemistry, Trinity College Dublin, Dublin 2, Ireland

⁴Department of Mechanical Engineering, University of Siegen, 57076 Siegen, Germany

⁵Wilhelm-Ostwald-Institute für Physikalische und Theoretische Chemie, Universität Leipzig, Linné Str. 2, 04103 Leipzig, Germany

⁶Infineon Technologies AG, Wernerwerkstraße 2, 93049 Regensburg, Germany

⁷Advanced Microelectronic Center Aachen (AMICA), AMO GmbH, Otto-Blumenthal-Str. 25, 52074 Aachen, Germany

KEYWORDS pressure sensors, platinum diselenide, PtSe₂, gauge factors, strain sensors

ABSTRACT: Two-dimensional (2D) layered materials are ideal for micro- and nanoelectromechanical systems (MEMS/NEMS) due to their ultimate thinness. Platinum diselenide (PtSe_2), an exciting and unexplored 2D transition metal dichalcogenides (TMD) material, is particularly interesting because its scalable and low temperature growth process is compatible with silicon technology. Here, we explore the potential of thin PtSe_2 films as electromechanical piezoresistive sensors. All experiments have been conducted with semi-metallic PtSe_2 films grown by thermally assisted conversion of Pt at a CMOS-compatible temperature of 400°C . We report high negative gauge factors of up to -84.8 obtained experimentally from PtSe_2 strain gauges in a bending cantilever beam setup. Integrated NEMS piezoresistive pressure sensors with freestanding PMMA/ PtSe_2 membranes confirm the negative gauge factor and exhibit very high sensitivity, outperforming previously reported values by orders of magnitude. We employ density functional theory (DFT) calculations to understand the origin of the measured negative gauge factor. Our results suggest PtSe_2 as a very promising candidate for future NEMS applications, including integration into CMOS production lines.

Layered two-dimensional (2D) materials have extraordinary electrical, optical and mechanical properties that suggest high potential for a wide range of nanoelectronics applications.^{1,2} 2D transition metal dichalcogenides (TMDs) have recently been intensively investigated due to their wide range of inherent electronic properties that complement graphene. Out of this family, platinum diselenide (PtSe₂) is a relatively new and thus far little explored TMD material. Monolayer PtSe₂ is a semiconductor with a band gap of 1.2 eV,³ while bulk PtSe₂ becomes semi-metallic with zero band gap.^{4,5} It has been grown epitaxially⁶ or synthesized on insulating substrates using thermally assisted conversion (TAC) of predeposited platinum (Pt) films by a vaporized solid selenium precursor.^{4,7} The latter process can be carried out at temperatures between 400 °C and 450 °C, which is compatible with standard semiconductor back end of line (BEOL) processing,⁸ in contrast to other 2D materials.^{9,10} We have demonstrated potential applications of TAC PtSe₂ in highly sensitive gas sensors and wide spectral photodetectors with equal or even superior performance compared to graphene and other TMD-based devices.^{7,11,12} Here, we explore the electromechanical properties of PtSe₂ in nanoelectromechanical (NEMS) pressure sensors. The devices utilize the piezoresistive effect in PtSe₂, which gives rise to a change in its electrical resistance upon mechanical strain. We investigate PtSe₂-membrane based pressure sensors and find sensitivities that are orders of magnitude higher than those of nanomaterial-based devices^{13–16}, including graphene^{17–19}. Furthermore, we obtain an average negative gauge factor (GF) of -84.8 for PtSe₂ from a bending beam setup. Detailed density functional theory (DFT) simulations reveal an increase in the density of states (DOS) at the Fermi level of bulk PtSe₂, corroborating the experimentally observed piezoresistive properties.

Polycrystalline PtSe₂ films with nanometer sized grains were grown on silicon/silicon dioxide (Si/SiO₂) substrates by TAC at 400 °C of predeposited 1 nm thick Pt films (Figure S1 in the

supporting information). Comprehensive characterization of layered PtSe₂ thin films synthesized in this manner, including X-ray photoelectron spectroscopy and scanning transmission electron microscopy is presented in our previous work.^{4,7,11} The thickness and roughness of the layers was determined by atomic force microscopy (AFM, Figure 1a,b). A thickness of 4.5 nm was found for the selenized 1 nm initial Pt film. Assuming an interlayer distance of 0.6 nm for PtSe₂²⁰, this corresponds to 7-8 layers for the 4.5 nm thick PtSe₂ film. The root mean square (RMS) roughness of the layer was 0.284 nm. The Raman spectrum of PtSe₂ film shows two sharp and prominent peaks corresponding to the E_g and A_{1g} modes of the 1T phase, attesting the crystalline nature of the films⁴ (Figure 1c). After the film growth, a polymethyl metacrylate (PMMA) was spin-coated on top of the PtSe₂.

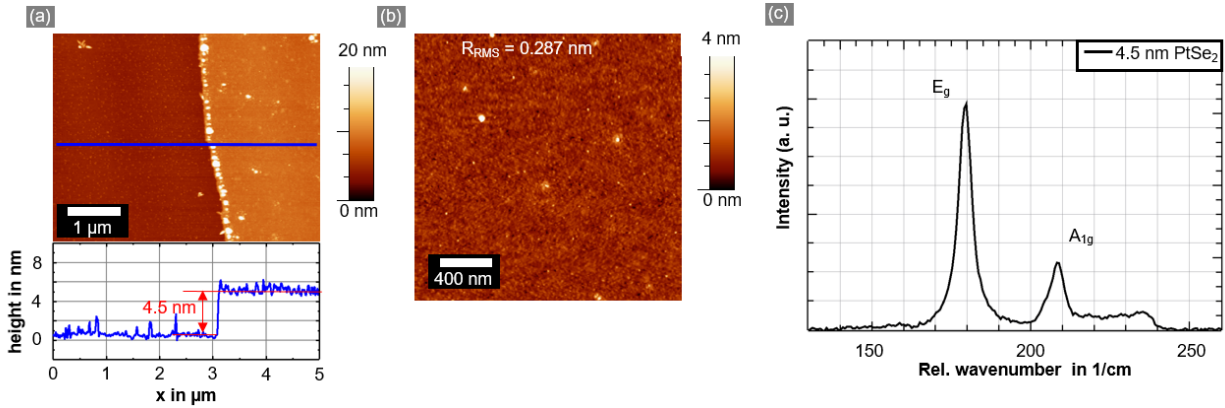


Figure 1. As-grown PtSe₂ film characterization: (a) AFM measurement of the selenized 1 nm initial Pt film including height profile of the step between the Si/SiO₂ substrate to the PtSe₂ film; (b) High-resolution AFM measurement displaying the RMS roughness; (c) Raman spectrum of the as-grown 4.5 nm thick PtSe₂ sample.

These centimeter-scale PtSe₂ thin films were transferred, using a typical polymer supported transfer process as described for graphene²¹, onto the substrate comprising of 79 independent pressure devices. Each device consists of cavities covered by a patterned PtSe₂ film located in

between metal contacts (Figure 2a-c). The PMMA layer was not removed after the transfer in order to stabilize and protect the PtSe₂ layer against environmental influences and to reduce possible cross sensitivity of the sensor. Details of the fabrication processes are described in the Experimental section and in the supporting information Figure S2a-d. A non-invasive Raman tomography cross-section, as demonstrated recently for graphene membranes,²² confirms the presence of free-standing PtSe₂ across the cavity (Figure 2d,e) where devices with suspended PtSe₂ (Figure 2e, top) and collapsed membrane (Figure 2e, bottom) were measured and can clearly be distinguished with this method. The corresponding spectrum of the suspended PtSe₂ shows the characteristic E_g and A_g modes without the Si(I) peak (Figure 2d, top), whereas the spectrum taken at the bottom of the trench shows only the characteristic Si(I) peak of the Si substrate (Figure 2d, bottom). This clear separation is feasible due to the 1.4 μ m deep cavity, which defines the distance between the suspended PtSe₂ and the Si substrate.

The operation of the investigated pressure sensors can be described in the following way: the PtSe₂/PMMA membranes seal the cavities and trap environmental pressure inside them.²³⁻²⁵ A different pressure (lower or higher) outside the cavity leads to deflection of the PtSe₂ membrane. This deflection induces strain in the PtSe₂ layer, resulting in a change of its resistance. The chip design used in the present experiments includes devices of similar size without cavities as control references. The pressure sensors, after wire-bonding and packaging into a chip socket, were placed in a home-built pressure chamber where pressure can be regulated from 1000 mbar (environmental pressure) down to 200 mbar (supporting information Figure S3). The pressure, humidity and temperature inside the chamber are recorded and controlled with commercial sensors during the experiments. Argon (Ar) atmosphere was used to exclude cross-sensitivity effects with gases and/or humidity.⁷ The current-voltage (I-V) characteristics of the PtSe₂ device for environmental pressure shows good linearity, i.e. the transferred PtSe₂ forms good Ohmic contacts with metal (copper) electrodes (supporting information Figure S4). The measured data is presented in Figure 2f along with the simultaneously measured pressure (dashed red line, right y-axis). The resistance across the PtSe₂ sensors decreases with applied increasing strain on the

membrane (caused by the decrease in pressure, supporting information Figure S5a). A pressure difference of 800 mbar between the outside and the inside of the cavity leads roughly to a 7% of change in resistance.

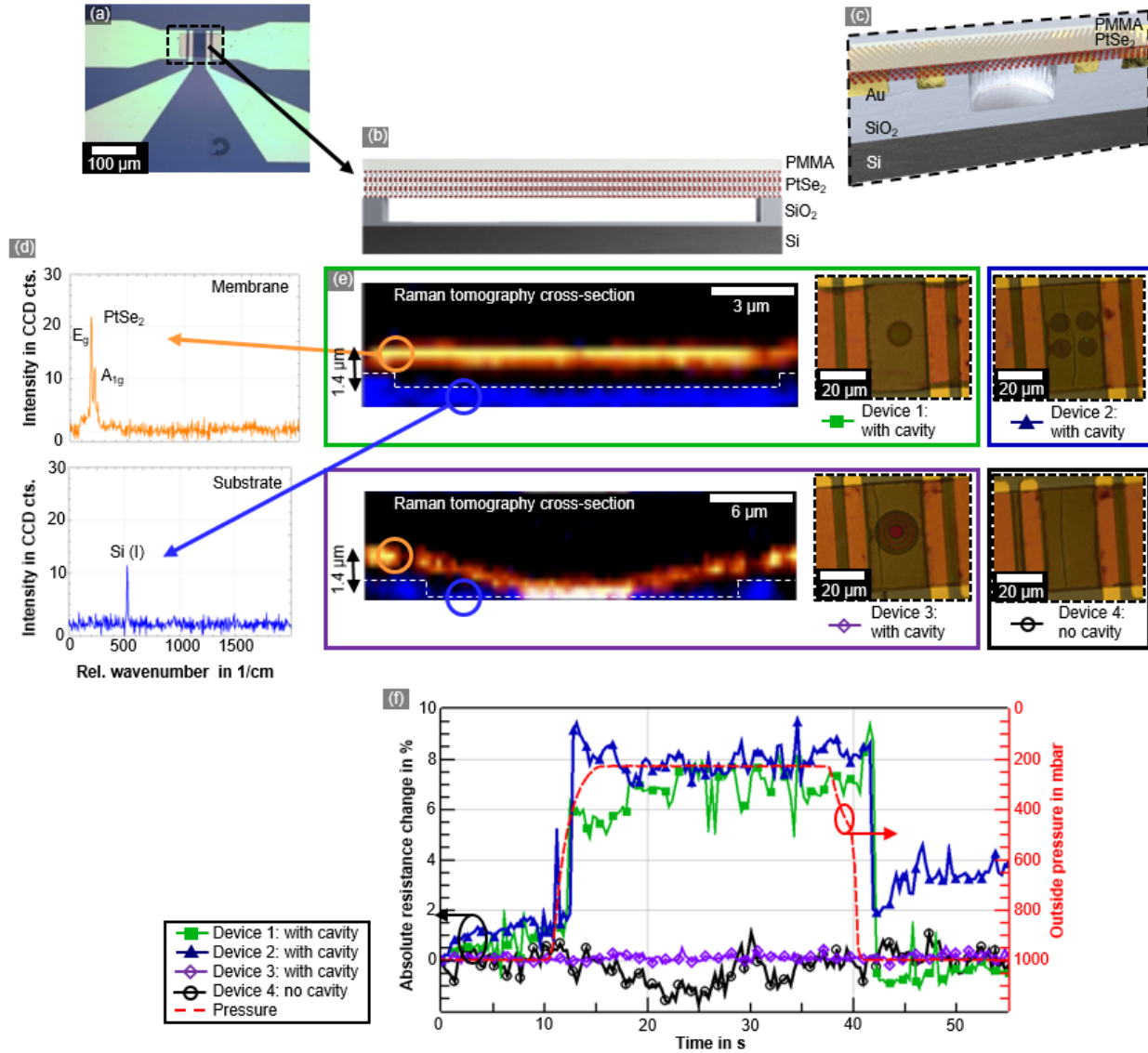


Figure 2. Pressure sensor fabrication and measurement. (a) Optical micrograph of one device with Au contacts and the PtSe₂ channel across the cavity area. (b) Schematic cross-section of the cavity area with suspended PtSe₂. (c) Schematic of one device including contacts and cavity area. (d) Raman point spectrum of the PtSe₂ membrane area and the Si substrate. (e) Raman tomography cross-sections of one device with suspended PtSe₂ (device 1) and one with collapsed

membrane (device 3). On the right are the corresponding optical micrographs of the cavity areas (device 1 and 3) as well as one other working device (device 2) and one device without cavity (device 4) as reference. (f) Resistance change in % for one pressure cycle (vented, pumped down to 200 mbar, vented) of the four devices shown in (e) (left y-axis) and the outside pressure (right y-axis).

The results of four devices are displayed in Figure 2f: two intact membranes on cavities (filled green squares and filled blue triangles), one with a collapsed membrane (empty purple diamond) and one for a reference device without cavity (empty black circles). A slight decrease (increase) in humidity during evacuation (venting) of the chamber is commonly observed for all measurements (supporting information Figure S5b), but does not give rise to any change in the resistance. Cross-sensitivity towards humidity can thus be excluded from having any substantial influence on the device behavior. We conclude that the observed resistance change is primarily caused by pressure (i.e. strain) changes during the measurements.

The absolute sensitivity (S) of a piezoresistive device is calculated using equation (1), where $\Delta R/R$ is the absolute value of the relative resistance change and ΔP is the pressure change during the sensor operation.¹⁷

$$S = \frac{\Delta R}{R \cdot \Delta P} \quad (1)$$

A total of 19 working devices were measured on four different chips through 69 different measurements (Figure 3a). A sensitivity of $1.05 \times 10^{-4} \text{ mbar}^{-1}$ was extracted from Figure 2f. An average of $5.51 \times 10^{-4} \text{ mbar}^{-1}$ was calculated for all measured devices (best device not included). The results were compared to some other NEMS pressure sensors which operate in a similar pressure range (Figure 3b,c). These use gallium arsenide (GaAs)²⁶, Si nanowires (Si NWs)^{14,15}, single- and multi-wall carbon nanotubes (SWNT and MWNT)^{13,16} and graphene¹⁷⁻¹⁹ as the piezoresistive materials. However, for most of these (except Smith *et al.*¹⁷ and Fung *et al.*¹⁶) a separate membrane is needed which is treated, or where the piezoresistive materials are grown or

applied, in a separate fabrication step. This adds additional complexity to the fabrication process, which is not the case for the PtSe₂-based pressure sensors, because the material acts as membrane and sensor at the same time. The thickness of other material is limited due to their mechanical stability. The measured sensitivity outperforms the best reported 2D and low dimensional materials based pressure sensors by a factor between 3 and 70 (Figure 3b). The SWNT-based pressure sensor¹³ shows an equal sensitivity, however the membrane areas are nearly two to four orders of magnitude larger than the PtSe₂ membrane. To take this into account the sensitivity can be normalized to the membrane area to receive a direct comparison between the devices independent of their membrane size^{27,17}. Here, the PtSe₂-based pressure sensor shows nearly 2 to 5 orders of magnitude higher sensitivity than the other devices (Figure 3c, see also supporting information Table S6).

We further point out that one of the devices showed an exceptionally high sensitivity of $1.64 \times 10^{-3} \text{ mbar}^{-1}$ (Figure S5c). Even though it could not be reproduced in other devices, this value was repeatedly measured for that particular device (Figure 3a, Chip 2, device 1). The sensitivity and normalized sensitivity of this device are plotted in Figure 3b,c (black star). When normalized to the membrane area, this device is over 3 orders of magnitude more sensitive than the highest performing devices shown in Figure 3c (a SWNT¹³ and a graphene membrane¹⁷ based device), and 4 to 6 orders of magnitude more sensitive than other reported devices.

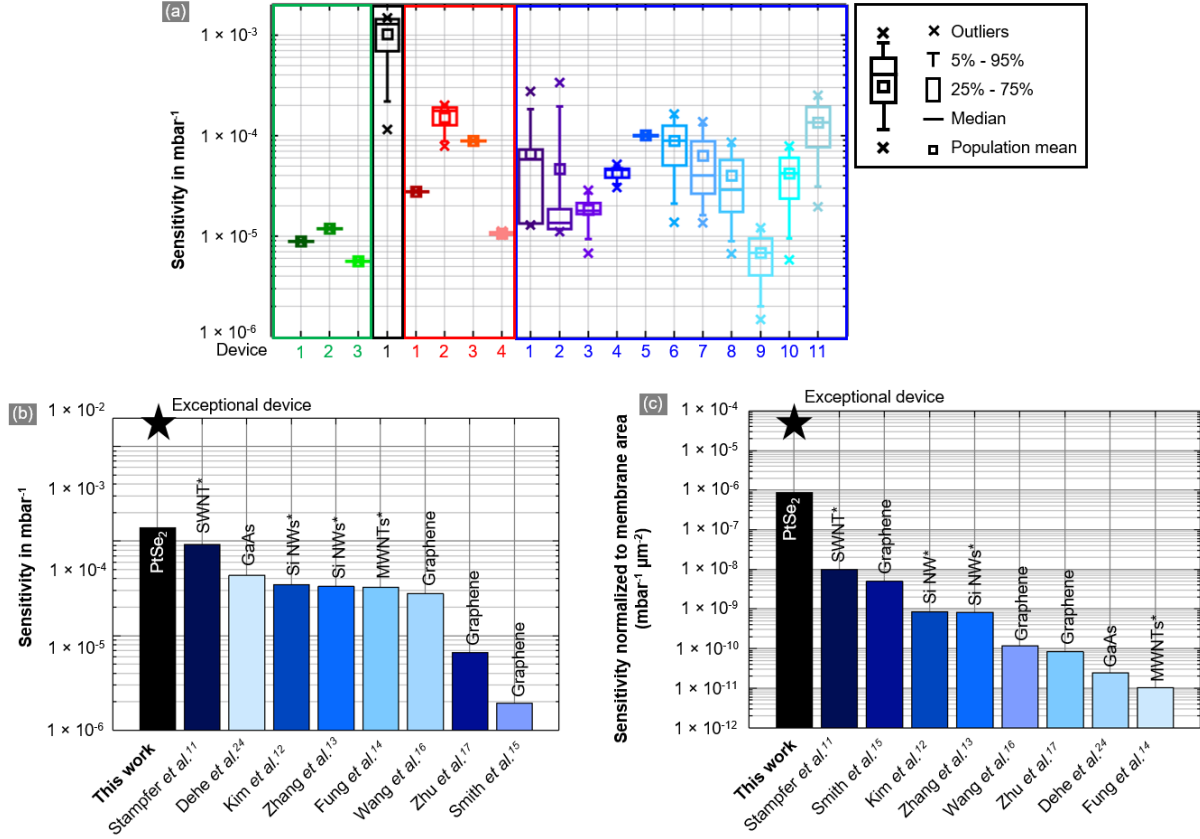


Figure 3. Comparison of all measured chips and devices as well as comparison of various pressure sensor devices using different materials for piezoresistive detection. (a) Box and whiskers plot of all measured chips, devices and repeated measurements; (b) Comparison of the sensitivity in mbar^{-1} with other pressure sensors; (c) comparison of the sensitivity normalized by membrane area in $\text{mbar}^{-1} \mu\text{m}^{-2}$ with other pressure sensors. In plots (b) and (c), devices which require a separate membrane are indicated with a * and the device with exceptionally high sensitivity is indicated by a black star.

A bending beam setup was used to measure another figure of merit, the piezoresistive gauge factor, of the 4.5 nm and 9 nm thick PtS_2 films which 7-8 and around 15 layers, respectively. The bending beam setup enables in a very simple way measurements of well-defined strain fields. The gauge factor (GF) can be extracted using equation (2).²⁸

$$GF = \frac{\Delta R}{R_0 \cdot \varepsilon} \quad (2)$$

Here, ε is the strain in the bending beam at the position of the sensor ($\varepsilon = 0.04\%$). A negative gauge factor (GF) of -84.8 was obtained (Figure 4a, supporting information section S7 and S9). The measured resistance change is shown in Figure 4b and in the supporting information Figure S9b for two PtSe₂ layer thicknesses, a mass of 2 kg (Figure 4b) and 0.5 kg (Figure S9c in the supporting information) and multiple cycles with a mass of 2 kg (Figure S9d in the supporting information). Data from a commercially available metal strain gauge is used as a reference (Figure 4b). A decrease in resistance with increasing strain on the PtSe₂ film corroborates the integrated pressure sensor measurements (supporting information Figure S9a). The GF of the PtSe₂ films exceeds the GF of the metal strain gauge (GF of 2)²⁸ and of graphene (GF of 2-5)^{23,29}. While similar or higher GF have been found for doped silicon (GF of -100 to +200)²⁸ or mono- and trilayer MoS₂ (GF of -148 and -43.5)³⁰.

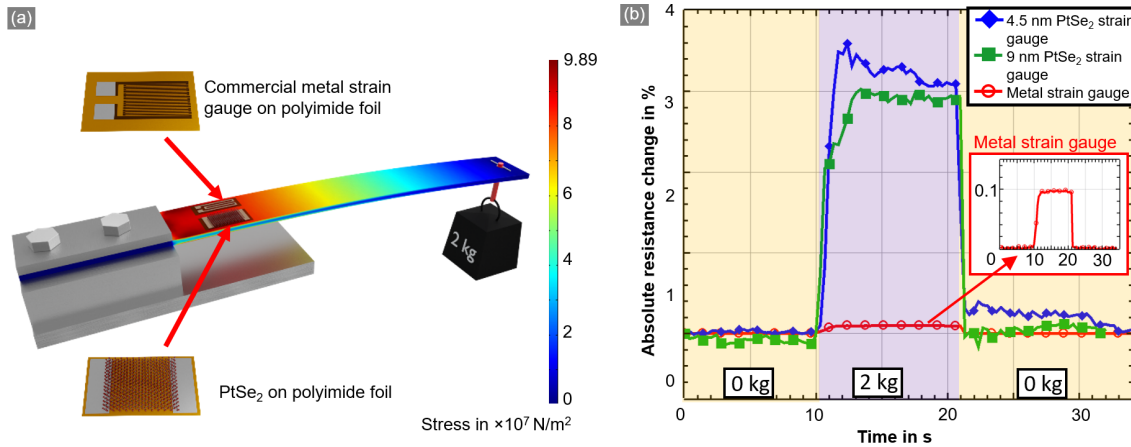


Figure 4. (a) Bending beam setup (cantilever beam) with applied PtSe₂ and commercially available metal strain gauges including stress simulation with the applied weight; (b) Electrical readout signal during the measurement with an absolute resistance change against time showing two PtSe₂ devices (of 4.5 nm PtSe₂, diamonds filled in blue and 9 nm PtSe₂, squares filled in

green) and a metal strain gauge (empty red circles) as reference with an enlarged view in the inset.

DFT calculations were conducted to gain insights into the observed resistance decrease with increased strain in PtSe_2 films. The model was fully optimized in terms of the lattice vectors and atomic positions. In the bulk system, which is similar to the experimental conditions in this work, biaxial strain means that the layers are stretched or compressed in plane. As bulk PtSe_2 is metallic, the DOS at the Fermi level is found to increase under biaxial tensile strain (ϵ_x) and reduces under compression, as shown in the supporting information Figure S10a. This result is in accordance with the experimental findings, where the resistivity decreases with increased ϵ_x .

Next, we have considered the effect of the interlayer strain and compression (ϵ_z) on the DOS. The results are shown in the supporting information Figure S10b. The compression of the interlayer distance has the opposite influence on the system and it slightly reduces the DOS at the Fermi level. Finally, we have considered the two effects acting in tandem in the following way: for in-plane stretching, there is a compression out of the plane, and vice versa (Figure 5a). The results for the combined effect are shown in Figure 5b. Once again, the DOS at the Fermi level is increased for the in plane stretching and compression in the out-of-plane direction. However, the effect is reduced compared to just ϵ_x , due to the opposite effect of the interlayer compression, as shown in the supporting information Figure S10b. In comparison to the significant increase of the DOS at the Fermi level upon strain the band structure shows only minor changes (Figure S10c in the supporting information) not indicating strong differences in the effective masses under strain.

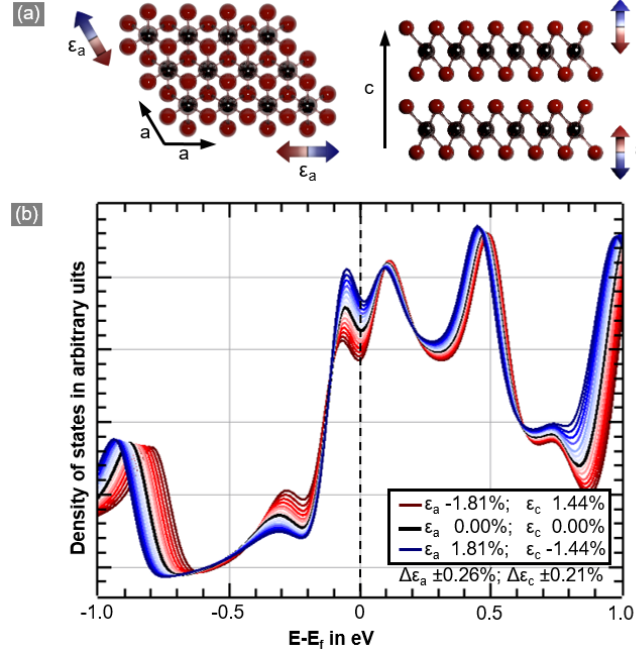


Figure 5. (a) Top and side view of the PtSe₂ bulk shown with the in-plane, a and out-of-plane, c lattice vectors, and the direction of the applied strain (ϵ_a and ϵ_c). (b) Density of states close to the Fermi level (shifted to zero) under applied tensile strain and compression.

An increase in DOS has also been reported for other single and few layer semiconducting TMDs, like MoS₂,³¹ MoSe₂,³² WSe₂,³² and also PtSe₂.³³ The semiconducting materials exhibit a decrease in band gap and even a transition to metallic behavior with applied strain, resulting in a negative gauge factor. For more detailed future studies the influence of many other parameters should be considered and investigated, including the adhesive interface between the steel beam and the polyimide foil, the thickness and mechanical properties of the foil and the PMMA layer covering the PtSe₂. Also, the crystallographic orientations, thickness and other material properties of the TAC-grown PtSe₂ film need to be investigated and considered in the simulations. Nevertheless, the results of the simulations show a clear indication of an increase in DOS, leading to a decrease in resistance under the applied strain, which is the most plausible cause of the experimentally extracted negative GF.

We have demonstrated PtSe₂-based piezoresistive pressure sensors with high gauge factors and very high sensitivity. The experiments were conducted on large-area PtSe₂ thin films grown by a scalable method of thermal conversion of metallic films at a low temperature of 400°C. A negative gauge factor of approximately -85 was obtained from a PtSe₂ strain gauge through bending beam experiments and can be understood in terms of a strain-induced increase in the density of states (DOS), as verified through DFT simulations. Furthermore, integrated piezoresistive pressure sensors were fabricated using PtSe₂/PMMA membranes. The PtSe₂ pressure sensors showed very high sensitivity, outperforming piezoresistive pressure sensors based on other materials by at least a factor of 82. When normalized to the active membrane area, the sensitivity of our devices is almost two to five orders of magnitude larger than reported values from any other technology till date. One exceptional device has an even higher sensitivity of $1.64 \times 10^3 \text{ mbar}^{-1}$ and outperforms existing technologies by an even greater margin. These results suggest that layered 2D PtSe₂ has great potential for future piezoresistive NEMS applications, beyond the demonstrated pressure sensors. These devices have a footprint that is up to four orders of magnitude smaller than other pressure sensors while showing a similar or even higher sensitivity. Further down-scaling to smaller cavities will improve the stability and yield of the membranes, and allow decreasing the membrane thickness to maintain the high sensitivity. The low growth temperature and general CMOS material compatibility makes PtSe₂ highly attractive for future silicon technology integration.

Methods

Materials Synthesis and analysis

Pt layers with a thickness of 1 and 2 nm were sputter deposited on $1.5 \times 1.5 \text{ cm}^2$ Si/SiO₂ substrates using a Gatan coating system (Gatan 682 PECS) with a 19 mm diameter Pt target. A TAC process was used to selenize the pre-deposited Pt layers, as described in detail in references.^{4,7} The cross-sectional Raman measurements were conducted using a WITec alpha 300R system with a 532 nm laser as source of excitation. A laser power of 75 μW was used. For obtaining single Raman spectra an 1800 g/mm grating was used, while the depth scan (cross-section) was conducted with a 300 g/mm grating. The system is limited to a lateral and vertical resolution of 300 nm and 900 nm, respectively.

Strain gauge fabrication

The strain gauges were fabricated by transferring as-grown PtSe₂ films onto pre-patterned polyimide foil substrates. A typical polymer-supported transfer method was used for the film transfer. 200 nm thick PMMA (Allresist AR-P 649.04) was spun on the as-grown PtSe₂ samples at a speed of 2000 rpm for 50 s. After spin-coating, the samples were annealed for 5 min at 80°C to cure the PMMA. 2 molar KOH was used to etch away the SiO₂ layer and release the PMMA-covered PtSe₂ films from the substrate. The PMMA-covered PtSe₂ films were cleaned in DI-water, followed by a transfer to the pre-patterned (500 nm thick copper contacts from evaporation) polyimide foil. After drying, the foil was glued (super glue Z70 by HBM) onto the steel beam (size of $300 \times 30 \text{ mm}^2$, 3 mm thick), 200 mm away from the loading point. A commercially available metal strain gauge was glued next to the PtSe₂ strain gauge. Cables were then soldered onto the contact pads for electrical connections.

Pressure sensor fabrication

A Si chip ($7 \times 7 \text{ mm}^2$) with 1.6 μm thick SiO₂ was used as a device substrate (Figure S2a in the supporting information). The cavities have circular geometry (radii between 2 μm and 20 μm)

with arrays of 1 to 15 cavities and rectangular geometries (length of 20 μm and width between 2 μm and 4 μm) in arrays between 1 and 3 cavities. They were structured by photolithography, followed by Ar- and CHF_3 -based reactive ion etching (RIE, 200 mW, 40 mTorr) to create a vertical profile with 1.4 μm of depth (Figure S2b in the supporting information). The contact regions were defined by photolithography, followed by a RIE process to embed the contacts and self-aligned metal evaporation (Cr/Au, 40 nm/400 nm, Figure S2c in the supporting information). The PtSe_2 films grown from 1 nm initial Pt films were transferred onto the device substrate using a PMMA-supported transport method as described above (Figure S2d in the supporting information). Lastly, the chip was wire bonded into a 44-pin PLCC chip package using 25 μm diameter Au wire.

Simulation

All calculations were performed using the DFT method as implemented in the VASP plane wave code.^{34,35} Ion-electron interactions were described by projector augmented wave approximation.³⁶ We have employed Perdew–Burke–Ernzerhof (PBE)³⁷ functional under the generalized gradient approximation. Van der Waals interaction corrections were included using the D3 approach proposed by Grimme.³⁸ Cutoff energy was set to 600 eV and the convergence threshold for residual force was 0.01 eV \AA^{-1} . Brillouin zone integration was carried out at 6 \times 6 \times 6 Monkhorst–Pack k-grids. Spin-orbit coupling (SOC) was included in the electronic structure calculations. Bulk PtSe_2 was fully optimized (lattice vectors and atomic positions) resulting in the following lattice vectors: $a = b = 3.788 \text{ \AA}$ and $c = 4.790 \text{ \AA}$, and a distance between Se atoms in the Se-Pt-Se sandwich of 2.550 \AA . This is in good agreement with the experimental data by Wang et al.,⁶ with $a = b = 3.70 \text{ \AA}$ and the distance between Se atoms of 2.53 \AA .

SUPPORTING INFORMATION

A schematic of the growth process for PtSe₂ is shown with additional Raman spectra and a TEM cross-section of the layered films. The fabrication process is described in a schematic and the measurement chamber is shown in a schematic. I-V characteristics of the unstrained pressure sensor are shown as well as additional electrical characterization data of the pressure sensors. A table compares pressure sensors from literature. The strain gauge measurements are described in detail, including the I-V characteristics of the devices as well as further electrical data. Further DFT calculations are shown for bulk and for three layer PtSe₂.

AUTHOR INFORMATION

Corresponding Author

*Tel: +49 241 8867 200, Email: max.lemme@eld.rwth-aachen.de; lemme@amo.de

Author Contributions

The manuscript was written through contributions of all authors. All authors have given approval to the final version of the manuscript.

ACKNOWLEDGMENT

Funding from the M-ERANET/German Federal Ministry of Education and Research (BMBF, NanoGraM, 03XP0006), the European Research Council (ERC, InteGraDe, 3017311), FLAG-ERA (HE 3543/27-1), European Union Seventh Framework Program: Graphene Flagship (Grant No. 649953), Science Foundation Ireland (PI Grant No. 15/IA/3131, 12/RC/2278 and 15/SIRG/3329) and the German Research Foundation (DFG LE 2440/1-2 and HE 3543/18-1) are gratefully acknowledged.

The authors would like to thank Anderson Smith for etching the cavities of the chips and for fruitful discussions and Martin Otto for conducting the AFM measurements. The ZIH Dresden is gratefully acknowledged for the computer time.

ABBREVIATIONS

CCR2, CC chemokine receptor 2; CCL2, CC chemokine ligand 2; CCR5, CC chemokine receptor 5; TLC, thin layer chromatography.

REFERENCES

- (1) Lemme, M. C.; Li, L.-J.; Palacios, T.; Schwierz, F. Two-Dimensional Materials for Electronic Applications. *MRS Bull.* **2014**, 39 (08), 711–718.
- (2) Gupta, A.; Sakthivel, T.; Seal, S. Recent Development in 2D Materials beyond Graphene. *Prog. Mater. Sci.* **2015**, 73, 44–126.
- (3) Wang, Y.; Li, L.; Yao, W.; Song, S.; Sun, J. T.; Pan, J.; Ren, X.; Li, C.; Okunishi, E.; Wang, Y.-Q.; et al. Monolayer PtSe₂, a New Semiconducting Transition-Metal-Dichalcogenide, Epitaxially Grown by Direct Selenization of Pt. *Nano Lett.* **2015**, 15 (6), 4013–4018.
- (4) O'Brien, M.; McEvoy, N.; Motta, C.; Zheng, J.-Y.; Berner, N. C.; Kotakoski, J.; Kenan Elibol; Pennycook, T. J.; Meyer, J. C.; Yim, C.; et al. Raman Characterization of Platinum Diselenide Thin Films. *2D Mater.* **2016**, 3 (2), 021004.
- (5) Zhang, W.; Qin, J.; Huang, Z.; Zhang, W. The Mechanism of Layer Number and Strain Dependent Bandgap of 2D Crystal PtSe₂. *J. Appl. Phys.* **2017**, 122 (20), 205701.
- (6) Wang, Y.; Li, L.; Yao, W.; Song, S.; Sun, J. T.; Pan, J.; Ren, X.; Li, C.; Okunishi, E.; Wang, Y.-Q.; et al. Monolayer PtSe₂, a New Semiconducting Transition-Metal-Dichalcogenide, Epitaxially Grown by Direct Selenization of Pt. *Nano Lett.* **2015**, 15 (6), 4013–4018.
- (7) Yim, C.; Lee, K.; McEvoy, N.; O'Brien, M.; Riazimehr, S.; Berner, N. C.; Cullen, C. P.; Kotakoski, J.; Meyer, J. C.; Lemme, M. C.; et al. High-Performance Hybrid Electronic Devices from Layered PtSe₂ Films Grown at Low Temperature. *ACS Nano* **2016**, 10 (10), 9550–9558.
- (8) Plummer, J. D. *Silicon VLSI Technology: Fundamentals, Practice, and Modeling*; Pearson Education India, 2009.
- (9) Kataria, S.; Wagner, S.; Ruhkopf, J.; Gahoi, A.; Pandey, H.; Bornemann, R.; Vaziri, S.; Smith, A. D.; Ostling, M.; Lemme, M. C. Chemical Vapor Deposited Graphene: From Synthesis to Applications. *Phys. Status Solidi A* **2014**, 211 (11), 2439–2449.
- (10) McCreary, K. M.; Hanbicki, A. T.; Jernigan, G. G.; Culbertson, J. C.; Jonker, B. T. Synthesis of Large-Area WS₂ Monolayers with Exceptional Photoluminescence. *Sci. Rep.* **2016**, 6, 19159.
- (11) Yim, C.; McEvoy, N.; Riazimehr, S.; Schneider, D. S.; Gity, F.; Monaghan, S.; Hurley, P. K.; Lemme, M. C.; Duesberg, G. S. Wide Spectral Photoresponse of Layered Platinum Diselenide-Based Photodiodes. *Nano Lett.* **2018**.
- (12) Yim, C.; Passi, V.; Lemme, M. C.; Duesberg, G. S.; Coileáin, C. Ó.; Pallecchi, E.; Fadil, D.; McEvoy, N. Electrical Devices from Top-down Structured Platinum Diselenide Films. *Npj 2D Mater. Appl.* **2018**, 2 (1), 5.
- (13) Stampfer, C.; Helbling, T.; Obergfell, D.; Schöberle, B.; Tripp, M. K.; Jungen, A.; Roth, S.; Bright, V. M.; Hierold, C. Fabrication of Single-Walled Carbon-Nanotube-Based Pressure Sensors. *Nano Lett.* **2006**, 6 (2), 233–237.
- (14) Kim, J. H.; Park, K. T.; Kim, H. C.; Chun, K. Fabrication of a Piezoresistive Pressure Sensor for Enhancing Sensitivity Using Silicon Nanowire. In *TRANSDUCERS 2009 - 2009 International Solid-State Sensors, Actuators and Microsystems Conference*; 2009; pp 1936–1939.
- (15) Zhang, J.; Zhao, Y.; Ge, Y.; Li, M.; Yang, L.; Mao, X. Design Optimization and Fabrication of High-Sensitivity SOI Pressure Sensors with High Signal-to-Noise Ratios Based on Silicon Nanowire Piezoresistors. *Micromachines* **2016**, 7 (10), 187.
- (16) Fung, C. K. M.; Zhang, M. Q. H.; Chan, R. H. M.; Li, W. J. A PMMA-Based Micro Pressure Sensor Chip Using Carbon Nanotubes as Sensing Elements. In *18th IEEE International Conference on Micro Electro Mechanical Systems, 2005. MEMS 2005*; 2005; pp 251–254.
- (17) Smith, A. D.; Niklaus, F.; Paussa, A.; Vaziri, S.; Fischer, A. C.; Sterner, M.; Forsberg, F.; Delin, A.; Esseni, D.; Palestri, P.; et al. Electromechanical Piezoresistive Sensing in Suspended Graphene Membranes. *Nano Lett.* **2013**, 13 (7), 3237–3242.

- (18) Wang, Q.; Hong, W.; Dong, L. Graphene “microdrums” on a Freestanding Perforated Thin Membrane for High Sensitivity MEMS Pressure Sensors. *Nanoscale* **2016**.
- (19) Zhu, S.-E.; Ghatkesar, M. K.; Zhang, C.; Janssen, G. C. a. M. Graphene Based Piezoresistive Pressure Sensor. *Appl. Phys. Lett.* **2013**, *102* (16), 161904.
- (20) Yan, M.; Wang, E.; Zhou, X.; Zhang, G.; Zhang, H.; Zhang, K.; Yao, W.; Lu, N.; Shuzhen Yang; Wu, S.; et al. High Quality Atomically Thin PtSe₂ Films Grown by Molecular Beam Epitaxy. *2D Mater.* **2017**, *4* (4), 045015.
- (21) Wagner, S.; Weisenstein, C.; Smith, A. D.; Östling, M.; Kataria, S.; Lemme, M. C. Graphene Transfer Methods for the Fabrication of Membrane-Based NEMS Devices. *Microelectron. Eng.* **2016**, *159*, 108–113.
- (22) Wagner, S.; Dieing, T.; Centeno, A.; Zurutuza, A.; Smith, A. D.; Östling, M.; Kataria, S.; Lemme, M. C. Noninvasive Scanning Raman Spectroscopy and Tomography for Graphene Membrane Characterization. *Nano Lett.* **2017**.
- (23) Smith, A. D.; Niklaus, F.; Paussa, A.; Schröder, S.; Fischer, A. C.; Sterner, M.; Wagner, S.; Vaziri, S.; Forsberg, F.; Esseni, D.; et al. Piezoresistive Properties of Suspended Graphene Membranes under Uniaxial and Biaxial Strain in Nanoelectromechanical Pressure Sensors. *ACS Nano* **2016**, *10* (11), 9879–9886.
- (24) Bunch, J. S.; Verbridge, S. S.; Alden, J. S.; van der Zande, A. M.; Parpia, J. M.; Craighead, H. G.; McEuen, P. L. Impermeable Atomic Membranes from Graphene Sheets. *Nano Lett.* **2008**, *8* (8), 2458–2462.
- (25) Dolleman, R. J.; Cartamil-Bueno, S. J.; Zant, H. S. J. van der; Steeneken, P. G. Graphene Gas Osmometers. *2D Mater.* **2017**, *4* (1), 011002.
- (26) Dehe, A.; Fricke, K.; Mutamba, K.; Hartnagel, H. L. A Piezoresistive GaAs Pressure Sensor with GaAs/AlGaAs Membrane Technology. *J. Micromechanics Microengineering* **1995**, *5* (2), 139.
- (27) Clark, S. K.; Wise, K. D. Pressure Sensitivity in Anisotropically Etched Thin-Diaphragm Pressure Sensors. *IEEE Trans. Electron Devices* **1979**, *26* (12), 1887–1896.
- (28) Window, A. L. *Strain Gauge Technology*; Elsevier Applied Science: London; New York, 1992.
- (29) Huang, M.; Pascal, T. A.; Kim, H.; Goddard, W. A.; Greer, J. R. Electronic–Mechanical Coupling in Graphene from in Situ Nanoindentation Experiments and Multiscale Atomistic Simulations. *Nano Lett.* **2011**, *11* (3), 1241–1246.
- (30) Manzeli, S.; Allain, A.; Ghadimi, A.; Kis, A. Piezoresistivity and Strain-Induced Band Gap Tuning in Atomically Thin MoS₂. *Nano Lett.* **2015**, *15* (8), 5330–5335.
- (31) Nayak, A. P.; Bhattacharyya, S.; Zhu, J.; Liu, J.; Wu, X.; Pandey, T.; Jin, C.; Singh, A. K.; Akinwande, D.; Lin, J.-F. Pressure-Induced Semiconducting to Metallic Transition in Multilayered Molybdenum Disulphide. *Nat. Commun.* **2014**, *5*, 3731.
- (32) Hosseini, M.; Elahi, M.; Pourfath, M.; Esseni, D. Very Large Strain Gauges Based on Single Layer MoSe₂ and WSe₂ for Sensing Applications. *Appl. Phys. Lett.* **2015**, *107* (25), 253503.
- (33) Li, P.; Li, L.; Zeng, X. C. Tuning the Electronic Properties of Monolayer and Bilayer PtSe₂ via Strain Engineering. *J. Mater. Chem. C* **2016**, *4* (15), 3106–3112.
- (34) Kresse, G.; Furthmüller, J. Efficiency of Ab-Initio Total Energy Calculations for Metals and Semiconductors Using a Plane-Wave Basis Set. *Comput. Mater. Sci.* **1996**, *6* (1), 15–50.
- (35) Kresse, G.; Furthmüller, J. Efficient Iterative Schemes for Ab Initio Total-Energy Calculations Using a Plane-Wave Basis Set. *Phys. Rev. B* **1996**, *54* (16), 11169–11186.
- (36) Blöchl, P. E. Projector Augmented-Wave Method. *Phys. Rev. B* **1994**, *50* (24), 17953–17979.
- (37) Perdew, J. P.; Burke, K.; Ernzerhof, M. Generalized Gradient Approximation Made Simple. *Phys. Rev. Lett.* **1996**, *77* (18), 3865–3868.
- (38) Grimme, S.; Ehrlich, S.; Goerigk, L. Effect of the Damping Function in Dispersion Corrected Density Functional Theory. *J. Comput. Chem.* **2011**, *32* (7), 1456–1465.

Supporting information

Highly sensitive electromechanical piezoresistive pressure sensors based on large-area layered PtSe₂ films

Stefan Wagner¹, Chanyoung Yim², Niall McEvoy³, Satender Kataria¹, Volkan Yokaribas⁴,
Agnieszka Kuc⁵, Stephan Pindl⁶, Claus-Peter Fritzen⁴, Thomas Heine⁵, Georg S. Duesberg^{2,3},
Max C. Lemme^{1,2,7*}

¹Chair of Electronic Devices, Faculty of Electrical Engineering and Information Technology, RWTH Aachen University, Otto-Blumenthal-Str. 2, 52074 Aachen, Germany

²Institute of Physics, EIT 2, Faculty of Electrical Engineering and Information Technology, Universität der Bundeswehr München, Werner-Heisenberg-Weg 39, 85577 Neubiberg, Germany

³Centre for Research on Adaptive Nanostructures and Nanodevices (CRANN), Advanced Materials and BioEngineering Research (AMBER) and School of Chemistry, Trinity College Dublin, Dublin 2, Ireland

⁴Department of Mechanical Engineering, University of Siegen, 57076 Siegen, Germany

⁵Wilhelm-Ostwald-Institute für Physikalische und Theoretische Chemie, Universität Leipzig, Linné Str. 2, 04103 Leipzig, Germany

⁶Infineon Technologies AG, Wernerwerkstraße 2, 93049 Regensburg, Germany

⁷Advanced Microelectronic Center Aachen (AMICA), AMO GmbH, Otto-Blumenthal-Str. 2, 52074 Aachen, Germany

*Tel: +49 241 8867 200, Email: max.lemme@rwth-aachen.de; lemme@amo.de

S1: PtSe₂ synthesis via a TAC process

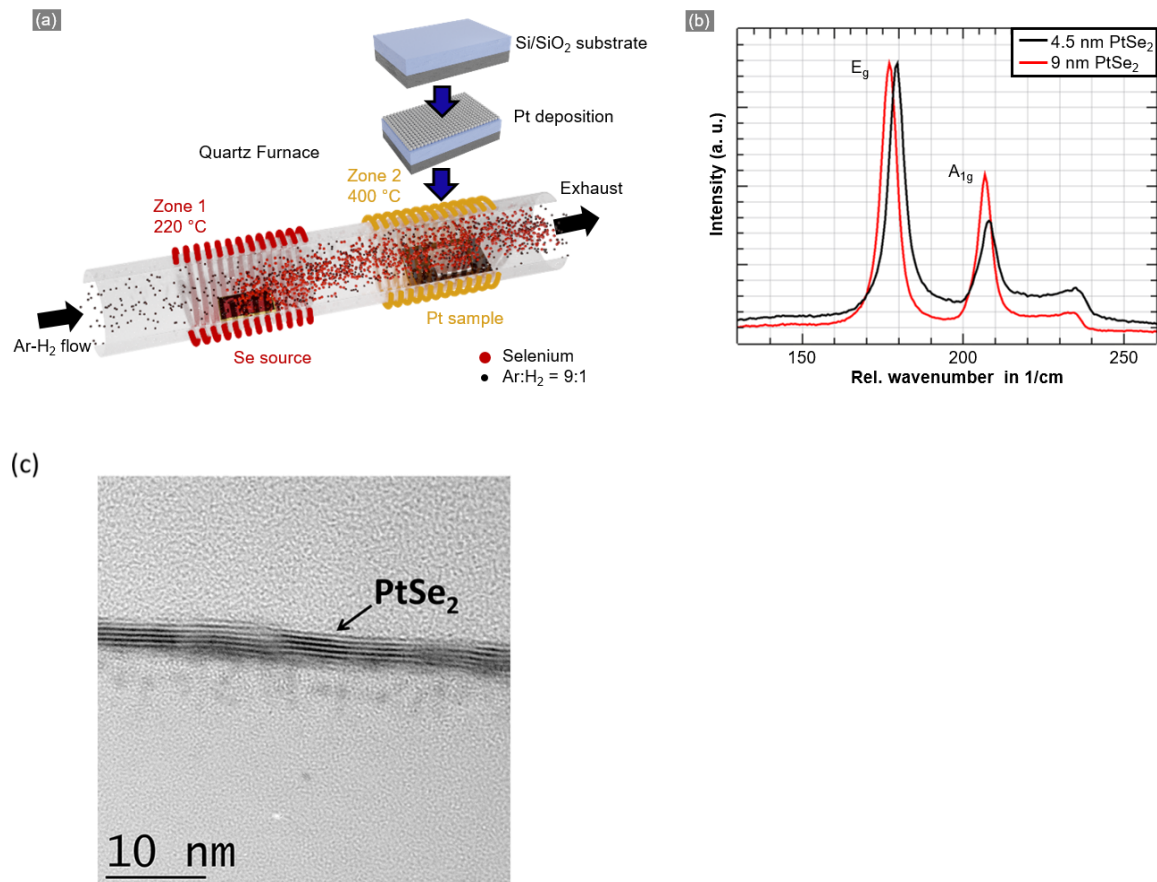


Figure S5: (a) Pt is deposited on a Si/SiO₂ substrate and placed into a quartz tube furnace. The Se source is evaporated in zone 1 at 220 °C and transported by the Ar-H₂ flow to zone 2, selenizing the Pt sample at 400 °C. (b) Raman spectra of 4.5 nm and 9 nm PtSe₂ films. (c) TEM cross-sectional image of a layered PtSe₂ film grown by TAC (adapted from ¹).

S2: Fabrication process of the pressure sensor

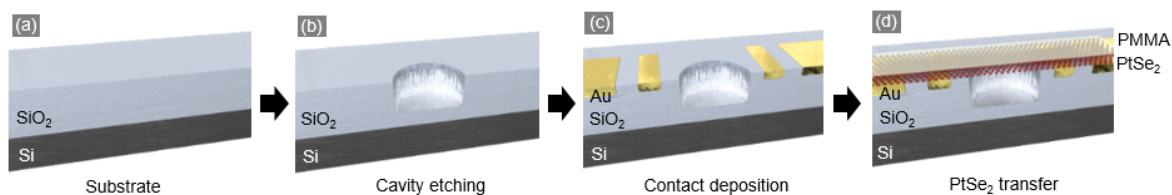


Figure S6: (a)-(d) A summary of the device fabrication process; (a) starting with a Si/SiO₂ substrate, (b) reactive ion etched (RIE) cavity, (c) the embedded metal contact deposition and (d) the transfer of PtSe₂ covered by a PMMA layer. See Methods for the detailed fabrication process description.

S3: Pressure chamber schematic

The chamber is built using standard vacuum components. Sensors included in the chamber are the humidity sensor HIH-4000 (Honeywell International Inc.), the temperature LM35 (Texas Instruments) sensor and the pressure sensor MXP2200AP (NXP Semiconductors).

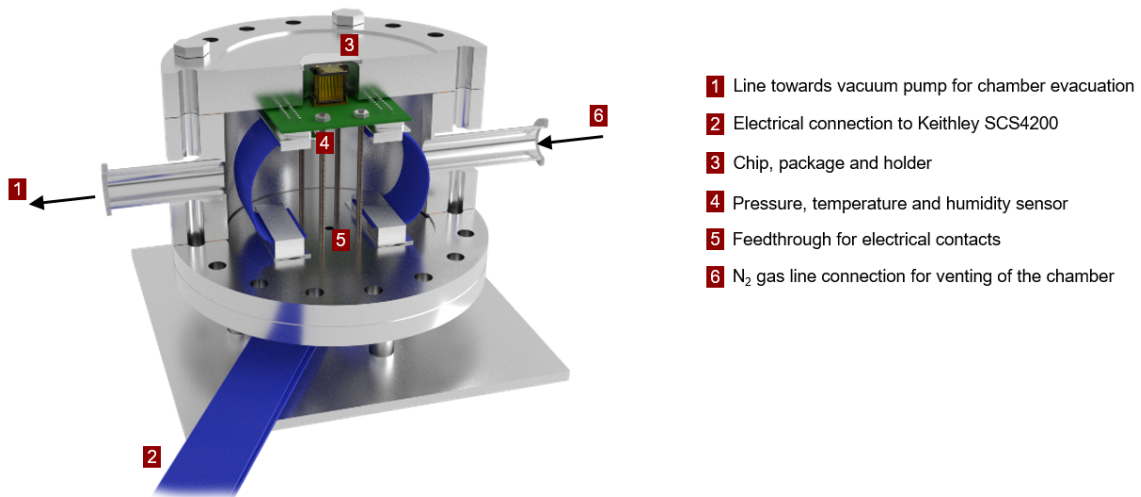


Figure S3: Home-built vacuum chamber design for the electrical measurement of NEMS pressure sensors.

S4: I-V curve at environmental pressure (unstrained)

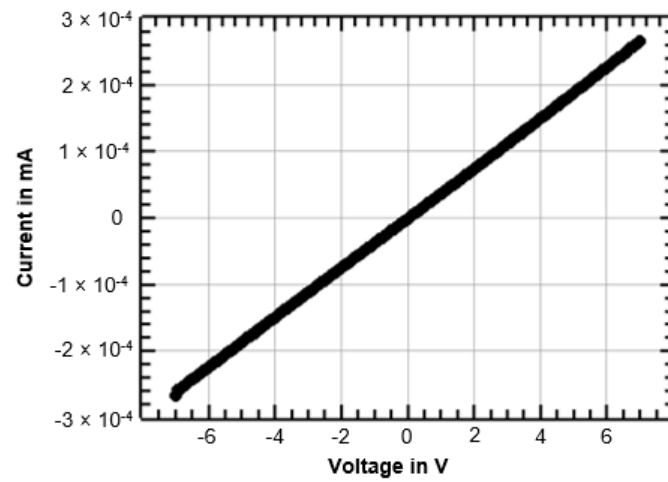


Figure S4: I-V curve of the PtSe₂ channel (1 nm initial Pt thickness) used as membrane for the pressure sensor at environmental pressure.

S5: Further measurements of the PtSe₂ pressure sensor

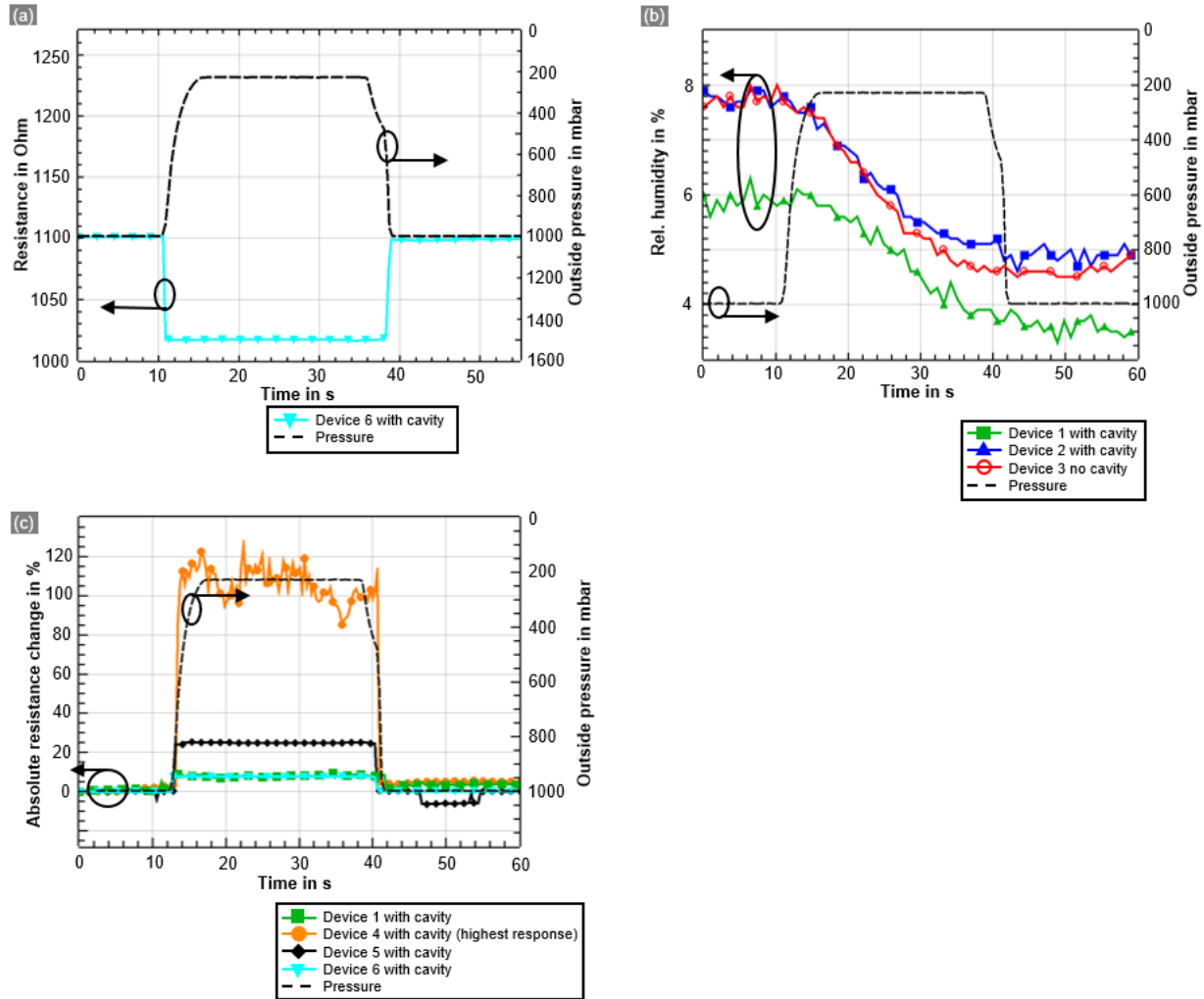


Figure S5: (a) Measured values plotted as resistance in Ohm against the time with a resistance decrease under strain with decreasing pressure of the PtSe₂ pressure sensor (triangles filled in turquoise); (b) Relative humidity of three devices (two devices with and one device without cavity as a reference) against the time with indicated pressure condition during measurement; (c) More measured devices with the resistance change in % (left y-axis) against the measurement time and the pressure during the experiment (right y-axis): device 1 for comparison, device 4 with the highest response detected and device 5 and 6 measured on a new chip with PtSe₂ from 1 nm starting Pt.

S6: Comparison of various pressure sensor devices

Table S1: Comparison of various pressure sensor devices ordered by the normalized sensitivity by membrane area.

Device structure	Membrane area (μm^2)	Sensitivity (mbar ⁻¹)	Sensitivity per membrane area (mbar ⁻¹ μm^{-2})	Publication year	References
Suspended PtSe2 covered with PMMA (exceptional device)	5.00E+01	1.64E-03	3.28E-05	2017	This work (highest value)
Suspended PtSe2 covered with PMMA	1.57E+02	1.39E-04	8.85E-07	2017	This work
SWNT	9.16E+03	9.26E-05	1.01E-08	2006	Stampfer et al. ²
Suspended Graphene	3.84E+02	1.94E-06	5.05E-09	2013	Smith et al. ³
Si nanowires	4.00E+04	3.47E-05	8.67E-10	2009	Kim et al. ⁴
Si nanowires	4.00E+04	3.33E-05	8.33E-10	2016	Zhang et al. ⁵
Suspended graphene on a perforated SiNx membrane	2.40E+05	2.80E-05	1.17E-10	2016	Wang et al. ⁶
Graphene on a suspended imperforated SiNx membrane	7.84E+04	6.67E-06	8.50E-11	2013	Zhu et al. ⁷
GaAs/AlGaAs	1.77E+06	4.37E-05	2.47E-11	1995	Dehe et al. ⁸
MWNT embedded into a PMMA diaphragm	3.14E+06	3.27E-05	1.04E-11	2005	Fung et al. ⁹

S7: PtSe₂ strain gauge

The PtSe₂ films were transferred onto a polyimide foil with prefabricated metal contacts to form a PtSe₂ strain gauge. The PMMA layer was left on the device to encapsulate the device and protect it against environmental influences, like humidity to avoid cross-sensitivity of the sensor and decrease the noise during the measurement. The strain gauge was then placed on a steel beam with known mechanical properties and glued at a position where high mechanical stress was expected (200 mm away from the point of load, main manuscript, Fig. 4a). Simulations of the stress distribution in the beam under load yield strain of about 0.04% at the sensing position, i.e. where PtSe₂ is fixed.¹⁰ With dimensions of the free beam (300 mm x 30 mm x 3 mm) and the distance between the sensing position and suspension point of the weight (200 mm), the stress (σ) which a sensor experiences, can be calculated from equation (S7.1, S7.2), where WT is the weight attached to the beam, x_m is the distance from the sensor to the suspension point, w is the beam width, t is the beam thickness, and E is the Young's modulus of the steel beam (0.2 TPa).

$$\sigma = \frac{WT \cdot x_m \cdot 6}{w \cdot t^2} \quad (\text{S7.1})$$

$$\varepsilon = \frac{\sigma}{E} \quad (\text{S7.2})$$

The calculated stress at the sensor is estimated to 8.71×10^7 N/m², therefore, a strain (ε) of 4.36×10^{-4} is extracted, which agrees well with the simulations.

A commercially available metal strain gauge was placed next to the PtSe₂ device as a reference. While a static bending beam experiment was conducted, the total resistance of the gauges was recorded at +1 V of dc bias. The current-voltage (I-V) characteristics of the PtSe₂ device for the unloaded case shows good linearity, i.e. the transferred PtSe₂ forms good Ohmic contacts with metal (copper) electrodes (supporting information, Fig. S8). The electrical response of the devices was measured during loading and unloading of a mass of 2 kg attached at the end of the cantilever beam. Fig. 4b of the main manuscript compares the absolute resistance change in percentage (%) for the PtSe₂ devices to a commercially available metal strain gauge over the measurement time. The applied strain causes a resistance change in the PtSe₂ films, implying the presence of a piezoresistive effect. The gauge factor has been calculated using equation (S7.3), where ΔR is the difference in resistance, R is the initial resistance in the unloaded case and ε is the strain.

$$GF = \frac{\Delta R}{R \cdot \varepsilon} \quad (S7.3)$$

The resistance of the PtSe₂ gauge decreases with applied strain, in contrast to a resistance increase of the metal strain gauge (supporting information, Fig. S9a). The electrical data result in an average negative GF of -84.8 for the PtSe₂ sensor. The GF of the commercial metal strain gauge is 2.1, in agreement with the specifications.¹⁰ The measurements were conducted for two different PtSe₂ thicknesses of 4.5 nm and 9 nm and repeated several times (supporting information, Fig. S9b). The measured devices highlight the consistent performance of the PtSe₂ film. The GF of these PtSe₂ layers is approximately 40 times higher than in metal¹⁰ and graphene,^{3,11} and comparable to MoS₂-based strain gauges.^{12,13} Due to its 2D nature, the PtSe₂-based strain gauge is believed to be more advantageous in flexible electronics than metal strain gauges suggesting high potential for applications in the area of wearable electronics.

S8: I-V curve of an unloaded strain gauge

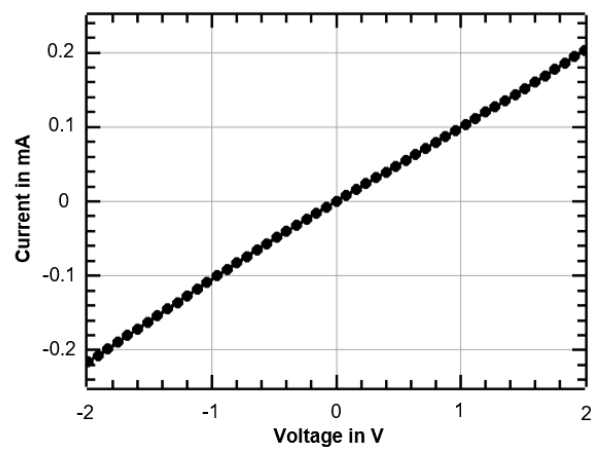


Figure S8: I-V curve of the PtSe_2 (4.5 nm thick PtSe_2) strain gauge for the unloaded case.

S9: Further measurements of the PtSe₂ strain sensor

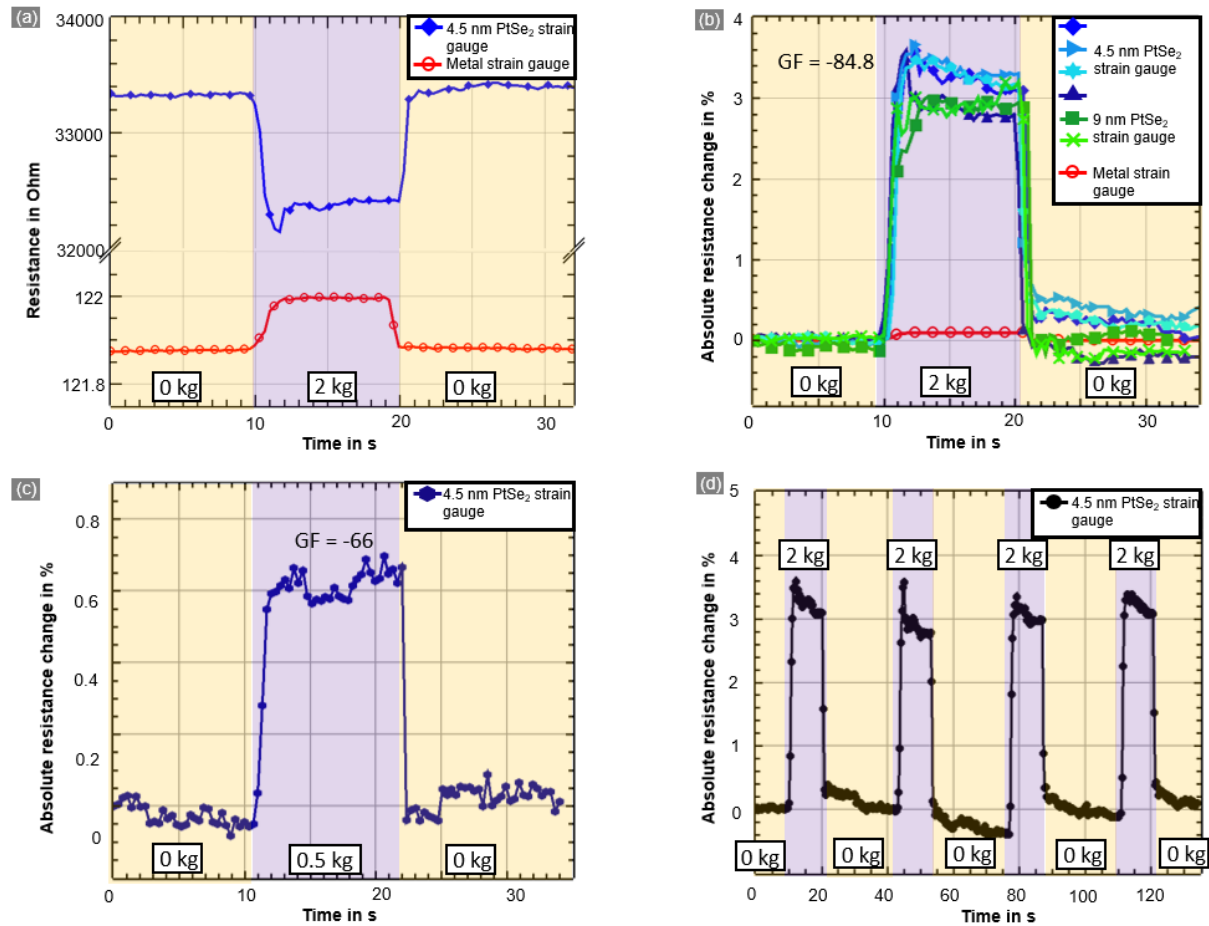


Figure S9: a) Measured values plotted as resistance in Ohm against the time with the metal strain gauge (empty circles with red outline), with a resistance increase under load and the PtSe₂ strain gauge (diamond filled in blue) with a resistance decrease under load; b) Plot of multiple measurements of the PtSe₂ strain gauges with PtSe₂ of 4.5 nm (shades of blue color) and 9 nm (shades of green color) thickness as well as the reference metal strain gauge (empty circles with red outline); (c) Bending beam measurement for a 4.5 nm thick PtSe₂ film and a mass of 0.5 kg; (d) Multiple cycles with a mass of 2 kg for a 4.5 nm thick PtSe₂ film.

S10: DFT calculations

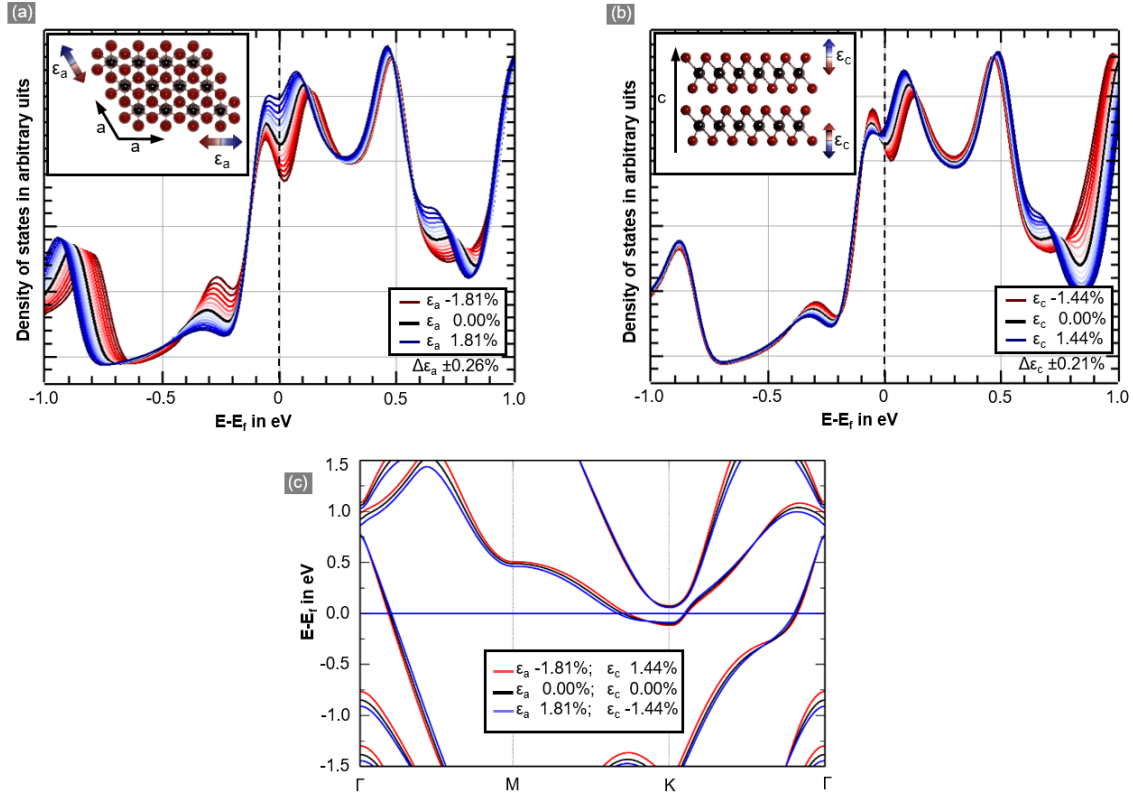


Figure S10: (a) Density of states close to the Fermi level (shifted to zero) under applied tensile strain and compression. The inset shows a top view of the PtSe₂ bulk with the in-plane lattice vector a and the direction of the biaxial strain (ϵ_a). (b) Density of states close to the Fermi level (shifted to zero) under applied tensile strain and compression. The inset shows the side view of the PtSe₂ bulk shown with the out-of-plane lattice vector c and the direction of the interlayer strain (ϵ_c); (c) the band structure of bulk PtSe₂.

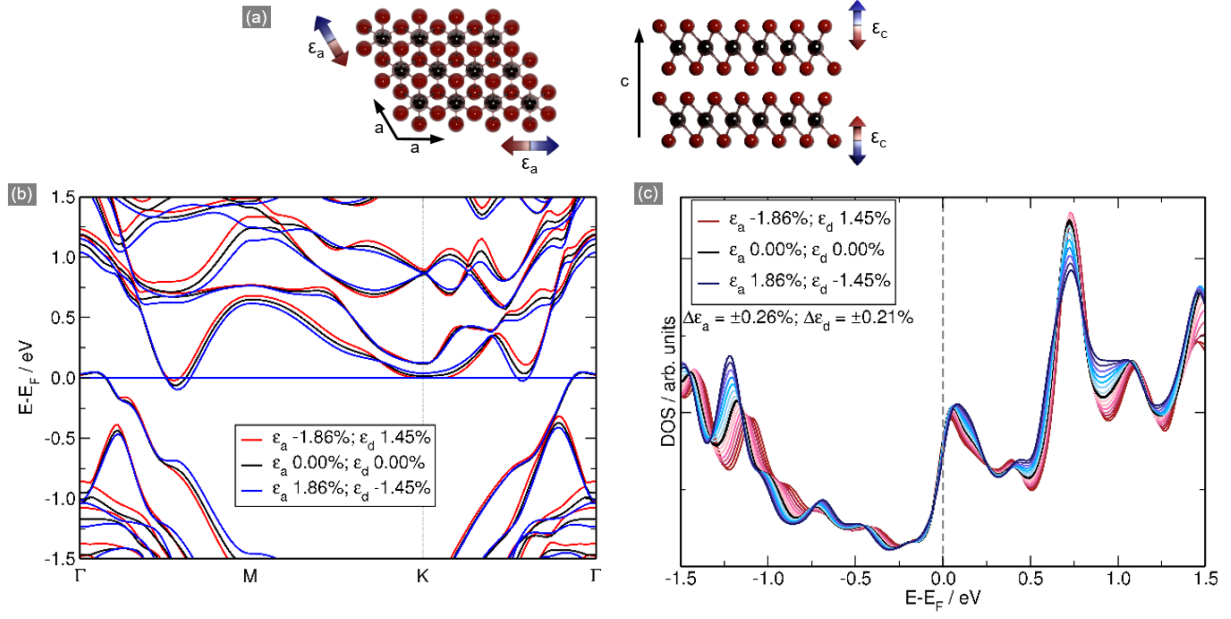


Figure S11: (a) Top and side view of the 3 layers PtSe₂ shown with the in-plane a and out-of-plane c lattice vectors, and the direction of the applied strain (ϵ_a and ϵ_c). (b) Band structure plot of 3 layers PtSe₂ under applied tensile and compressive strain; (c) Density of states close to the Fermi level (shifted to zero) under applied tensile strain and compression for 3 layers PtSe₂.

References:

- (1) Yim, C.; McEvoy, N.; Riazimehr, S.; Schneider, D. S.; Gity, F.; Monaghan, S.; Hurley, P. K.; Lemme, M. C.; Duesberg, G. S. Wide Spectral Photoresponse of Layered Platinum Diselenide-Based Photodiodes. *Nano Lett.* **2018**.
- (2) Stampfer, C.; Helbling, T.; Obergfell, D.; Schöberle, B.; Tripp, M. K.; Jungen, A.; Roth, S.; Bright, V. M.; Hierold, C. Fabrication of Single-Walled Carbon-Nanotube-Based Pressure Sensors. *Nano Lett.* **2006**, 6 (2), 233–237.
- (3) Smith, A. D.; Niklaus, F.; Paussa, A.; Vaziri, S.; Fischer, A. C.; Sterner, M.; Forsberg, F.; Delin, A.; Esseni, D.; Palestri, P.; et al. Electromechanical Piezoresistive Sensing in Suspended Graphene Membranes. *Nano Lett.* **2013**, 13 (7), 3237–3242.
- (4) Kim, J. H.; Park, K. T.; Kim, H. C.; Chun, K. Fabrication of a Piezoresistive Pressure Sensor for Enhancing Sensitivity Using Silicon Nanowire. In *TRANSDUCERS 2009 - 2009 International Solid-State Sensors, Actuators and Microsystems Conference*; 2009; pp 1936–1939.
- (5) Zhang, J.; Zhao, Y.; Ge, Y.; Li, M.; Yang, L.; Mao, X. Design Optimization and Fabrication of High-Sensitivity SOI Pressure Sensors with High Signal-to-Noise Ratios Based on Silicon Nanowire Piezoresistors. *Micromachines* **2016**, 7 (10), 187.
- (6) Wang, Q.; Hong, W.; Dong, L. Graphene “microdrums” on a Freestanding Perforated Thin Membrane for High Sensitivity MEMS Pressure Sensors. *Nanoscale* **2016**.
- (7) Zhu, S.-E.; Ghatkesar, M. K.; Zhang, C.; Janssen, G. C. a. M. Graphene Based Piezoresistive Pressure Sensor. *Appl. Phys. Lett.* **2013**, 102 (16), 161904.
- (8) Dehe, A.; Fricke, K.; Mutamba, K.; Hartnagel, H. L. A Piezoresistive GaAs Pressure Sensor with GaAs/AlGaAs Membrane Technology. *J. Micromechanics Microengineering* **1995**, 5 (2), 139.
- (9) Fung, C. K. M.; Zhang, M. Q. H.; Chan, R. H. M.; Li, W. J. A PMMA-Based Micro Pressure Sensor Chip Using Carbon Nanotubes as Sensing Elements. In *18th IEEE International Conference on Micro Electro Mechanical Systems, 2005. MEMS 2005*; 2005; pp 251–254.
- (10) Hoffmann, K. *Eine Einführung in Die Technik Des Messens Mit Dehnmessstreifen*; Hottinger Baldw, 1987.
- (11) Huang, M.; Pascal, T. A.; Kim, H.; Goddard, W. A.; Greer, J. R. Electronic–Mechanical Coupling in Graphene from in Situ Nanoindentation Experiments and Multiscale Atomistic Simulations. *Nano Lett.* **2011**, 11 (3), 1241–1246.
- (12) Wu, W.; Wang, L.; Li, Y.; Zhang, F.; Lin, L.; Niu, S.; Chenet, D.; Zhang, X.; Hao, Y.; Heinz, T. F.; et al. Piezoelectricity of Single-Atomic-Layer MoS₂ for Energy Conversion and Piezotronics. *Nature* **2014**, 514 (7523), 470–474.
- (13) Manzeli, S.; Allain, A.; Ghadimi, A.; Kis, A. Piezoresistivity and Strain-Induced Band Gap Tuning in Atomically Thin MoS₂. *Nano Lett.* **2015**, 15 (8), 5330–5335.